INTERNATIONAL ATOMIC ENERGY AGENCY
UNITED NATIONS EDUCATIONAL, SCIENTIFIC AND CULTURAL ORGANIZATION
INTERNATIONAL CENTRE FOR THEORETICAL PHYSICS
I.C.T.P., P.O. BOX 586, 34100 TRIESTE, ITALY, CABLE: CENTRATOM TRIESTE

SMR/382- 37

WORKSHOP ON SPACE PHYSICS:
"Materials in Microgravity"
27 February - 17 March 1989

"Interfacial Transport in Crystal Growth, a Parametric Comparison of Convective Effects"

F. ROSENBERGER
Centre for Microgravity Research
Huntsville, Alabama
USA

Journal of Crystal Growth 65 (1983) 91–104
North-Holland, Amsterdam

INTERFACIAL TRANSPORT IN CRYSTAL GROWTH, A PARAMETRIC COMPARISON OF CONVECTIVE EFFECTS

Franz ROSENBERGER

Department of Physics, University of Utah, Salt Lake City, Utah 84112, USA

and

Georg MÜLLER

Institut für Werkstoffwissenschaften VI, Universität Erlangen–Nürnberg, Martensstrasse, D-8520 Erlangen, Fed. Rep. of Germany

Most solid-state devices utilize properties of crystals obtained through the controlled introduction into the host lattice of impurities ("dopants") or deviations from stoichiometry. This compositional adjustment is typically made during the growth of the solid from its nutrient (melt, vapor or solution). Since the yield and performance of devices depends strongly on their compositional uniformity, a detailed understanding of the fluid dynamics of nutrient phases and at solid–nutrient interfaces is important. Rigorous modeling of heat and mass transfer in multicomponent (crystal growth) fluids for realistic boundary conditions is typically unwieldy. Hence, the motivation for simplification is great. Numerous simplifying models have been used in the materials preparation literature. Though well justified for some special cases, these concepts have been indiscriminately generalized, causing much confusion. In this presentation we take the opposite route. Based on the generally valid transport equations and the appropriate dimensionless groups of fluid properties, we point out (a) limitations of the most commonly used mass transfer models, and (b) physically justifiable analogies between mass, heat and momentum transfer. From these considerations one can get valuable semi-quantitative guidance for the laboratory practice in many situations that currently defy rigorous treatment.

1. Introduction

Most solid-state devices utilize properties of solids obtained through the controlled introduction into a host lattice of impurities ("dopants") or deviations from stoichiometry. The performance of such devices depends often strongly on the compositional homogeneity obtained. For instance, in modern microcircuitry, compositional variations of a few percent down to a submicron length scale can seriously jeopardize production yields. The compositional adjustment in solid components (crystals) is often made during their growth from the nutrient (melt, vapor or solution). Hence, a detailed understanding of the dynamics of mass transfer in nutrients at growing interfaces has become important.

Systems in which the solid possesses exactly the same composition as the nutrient from which it grows, i.e. congruently growing materials, are relatively rare. In most systems the property-determining component is either partly rejected by the advancing solid–nutrient interface, or the component becomes enriched in the solid. This can be described in terms of a segregation (distribution) coefficient, $k_0 = C_0^s/C_0^n$, where C^s and C^n stand for the concentration of the dopant or incongruent host component in the solid and nutrient, respectively. The subscript zero refers to values taken at the location of the interface, $x = 0$. Note that k_0 can only be equivalent to the equilibrium or thermodynamic segregation coefficient k^* if the interfacial growth and segregation kinetics is rapid as compared to the transport kinetics in the contacting bulk phases. This is not always the case.

At low growth rates and, hence, low interfacial segregation rates, the dopant concentration in the nutrient will be close to uniform, as schematically indicated in fig. 1a for a host-dopant combination with $k_0 < 1$. At practically feasible growth rates,

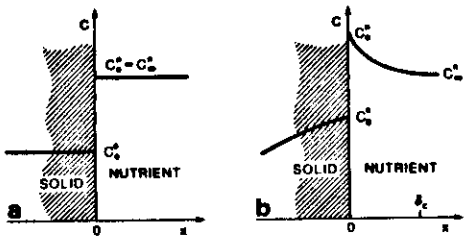

Fig. 1. Segregation at the solid–nutrient interface of a binary system: concentration profiles for dopant with segregation coefficient $k_0 < 1$ for (a) very small and (b) higher growth rate.

however, C_0^n becomes larger than the bulk value C_∞^n (fig. 1b). In terms of a segregation coefficient that is defined with respect to the more or less uniform concentration in the bulk nutrient, $k_{eff} = C_0^s/C_\infty^n$, one can express this increase as $k_0 < k_{eff} < 1$. The actual value of k_{eff} depends in a complex manner on the mass and heat transfer conditions at the interface and on the coupled growth rate.

This dynamic nature of C_0^s, per se, does not pose any problem in the control of doping levels. However, the transport conditions (diffusive–convective fluxes) are rarely uniform across the whole interface. For instance, convection at parts of a crystal that are close to a container wall is often less significant than at "more exposed" parts. Thus the composition becomes non-uniform parallel to the interface. Furthermore, any non-steady transport conditions, as they modify C_0^n, can lead to non-uniformities in the crystal composition normal to the interface, that are superimposed on the steady-state inhomogeneities. Even for perfectly stable external boundary conditions (e.g. furnace temperature), non-steady transport conditions can arise from time-dependent, buoyancy- or surface tension-driven convection in a nutrient. Therefore the materials science community has developed great interest in the low-gravity conditions obtainable in space crafts, that allow for a minimization of the buoyancy-driven convection and better defined studies of nutrient motion due to surface tension gradients.

Besides their influence on the segregation dynamics, concentration and temperature profiles at interfaces govern also the morphological stability of a growing crystal. This, again, is a complex topic. But in general, one can say that the probability for a solid–nutrient interface to loose its shape stability increases with increasing interfacial concentration gradients. Interfacial temperature gradients, $dT/dx > 0$, on the other hand, tend to stabilize interfaces.

From these introductory considerations it should be obvious that for both, the attainment of homogeneous solids as well as the achievement of high, stable growth rates, a quantitative description of the fluid dynamics of nutrients under physical and chemical conditions relevant to materials preparation is of great importance.

2. The governing equations

Rigorous modeling of heat and mass transfer in multicomponent (crystal growth) fluids requires the *simultaneous* solution of the conservation equations [1] for:

– momentum (Navier–Stokes equation, Newton's second law),

$$\underbrace{\frac{\partial}{\partial t}\rho v}_{\text{rate of change of momentum}} \underset{\text{from}}{=} \underbrace{-[\nabla\cdot\rho vv]}_{\text{convection}} - \underbrace{\nabla p}_{\text{pressure force}} \underbrace{-[\nabla\cdot\tau]}_{\text{viscous transfer}} + \underbrace{\rho g}_{\text{gravity or other body forces}}; \quad (1)$$

– mass (continuity equation),

$$\frac{\partial}{\partial t}\rho = -\nabla\cdot\rho v; \quad (2)$$

– species (e.g., binary diffusion equation), with i = A, B,

$$\underbrace{\frac{\partial}{\partial t}\rho_i}_{\text{rate of gain of mass}} \underset{\text{from}}{=} -\nabla\cdot\rho_i v_i = -[\underbrace{\nabla\cdot\rho_i v}_{\text{convection}} - \underbrace{\nabla\cdot\rho D_{AB}\nabla W_i}_{\text{diffusion}}]; \quad (3)$$

– energy

$$\underbrace{\frac{\partial}{\partial t}\rho\left(u+\frac{1}{2}v^2\right)}_{\substack{\text{rate of change}\\ \text{in internal and}\\ \text{kinetic energy}}} \underset{\text{from}}{=} \underbrace{-\left[\nabla\cdot\rho v\left(u+\frac{1}{2}v^2\right)\right]}_{\text{convection}} - \underbrace{(\nabla\cdot q)}_{\text{conduction}} - \underbrace{(\nabla\cdot pv)}_{\substack{\text{pressure}\\ \text{force}}} - \underbrace{(\nabla\cdot[\tau\cdot v])}_{\substack{\text{viscous}\\ \text{force}}} + \underbrace{\rho(v\cdot g)}_{\substack{\text{gravity}\\ \text{force}}}, \quad (4)$$

for typically rather complicated boundary conditions. (A list of nomenclature is given at the end of the paper.) We also have to consider the thermal equation of state $p = p(\rho_i, T)$, the caloric equation of state $u = u(\rho_i, T)$. Then we need expressions for the viscous momentum flux $\nabla\cdot\tau$ and the conductive heat flux q in terms of their driving gradients and transport coefficients. For systems with large disparities in the molecular weight of species, Soret diffusion must be added to the concentration diffusion term in (3). Chemical reactions introduce additional conditions. Radiative heat transfer, often dominant in materials processing, needs to be included in (4). Also, when strong component (interdiffusion) fluxes exist, (4) must be supplemented with a "diffusion-thermo" or Dufour flux term. This complete description then determines the concentration, velocity and temperature distributions as a function of the spatial coordinates and time.

Such a general formulation of transport is unwieldy and has been solved to date only for a few idealized (crystal growth) situations. Hence, the motivation for simplification is great. Numerous simplifying models have been used in the materials preparation literature. Though well justified for some special cases, these concepts have been indiscriminately generalized, causing much confusion. In the following we will take the opposite route. Based on the generally valid equations and the appropriate *dimensionless groups* of fluid properties and boundary conditions we will discuss the limitations of the most commonly used mass transfer models. Beyond that we will draw physically justifiable analogies to similar heat and momentum transport situations. Since these are experimentally more readily accessible than concentration distributions, valuable guidance for laboratory practice can be obtained from such analogies. Since our emphasis is on a comparison of different classes of nutrients, we will limit the discussion mostly to one-dimensional models.

3. Steady transport at interfaces

3.1. Diffusive-advective mass transport

The formal treatment of so-called purely diffusive transport is among the most controversial topics in the materials preparation literature. First, it is often overlooked that the specific form of (3) is based on the mass average velocity v and the mass fraction W_i. If other concentration coordinates (mole fraction, etc.) and/or reference velocities (mole average velocity, etc.) are used, other factors (than ρ) appear in the "Fick's first law" term of (3) (see e.g. refs. [2, 3]). This has been an inexhaustable source of errors – and of more or less clearly presented tutorials.

A second, closely related difficulty stems from a widespread misunderstanding of the definition of diffusive fluxes. Diffusion is in general understood as the component flux with respect to an average velocity of the system. Therefore the total mass flux of, say, component A in a binary system is

$$n_A = \rho_A v_A = \rho_A v + \rho D_{AB}\nabla W_A, \quad (5)$$

where the two terms on the rhs represent the convective and diffusive mass flux contributions, and the mass average velocity,

$$v = \frac{1}{\rho}\sum\rho_i v_i, \quad (6)$$

was chosen as average velocity. For other choices of the average velocity and the resulting different formulations of the diffusive flux term, see refs. [2,3]. In the absence of free or forced convection it has become customary to set the convective term in (5) equal to zero. On segregation at an interface, however, the mass average velocity, even in the absence of "conventional" convection, is typically nonzero. For instance, for a two component system in solution growth, assuming that the solvent

B is quantitatively rejected at the interface (considered stationary), in the one-dimensional treatment $v_B = 0$. Thus, one obtains from (6) $v = W_A v_A$ and for the "convective" term in (5)

$$\rho_A v = \rho_A W_A v_A = n_A W_A. \tag{7}$$

As the term "convective" is suggestive of free or forced flow we prefer to denote the diffusion-induced bulk flow (7) as *advective*. Note that the mass average velocity in the governing equations (1)–(4) contains both the externally caused bulk flow and the advective flow velocity contributions. Substitution of (7) into (5) yields for the "purely diffusive" component (diffusive–advective) mass flux towards a growing crystal

$$n_A = \frac{\rho D_{AB}}{1 - W_A} \frac{dW_A}{dx}, \tag{8}$$

rather than the widely used

$$n_A = \rho D_{AB}\, dW_A/dx. \tag{9}$$

From (8) we see that the advective flux term (7) "set up by diffusion" and thus the difference between (8) and (9) is significant whenever the concentration of the diffusant A is not too low. Consequently (9) forms an excellent approximation in many melt segregation problems with low dopant levels. Indiscriminate applications of (9) to high concentration solution growth or vapor growth, however, has lead to some rather amusing conclusions. The relation for mole fluxes corresponding to (8) was already clearly understood by Stefan in 1882 [4]. Consequently, advective flow velocities associated with diffusion are frequently referred to as Stefan velocities. Detailed discussions of this topic can be found in refs. [3,5,6].

3.2. Diffusive–convective mass transport

For a discussion of the relative weight of diffusive and convective (including advective) mass transfer and a comparison with energy and momentum transport, it is advantageous to rewrite (3) in terms of dimensionless parameters. In doing so, one refers to characteristic magnitudes of the variables. Based upon a characteristic (forced or free flow) velocity U_0 (or U_∞) and a characteristic length L one introduces the dimensionless ratios for

$$\text{velocity} \quad U = v/U_0; \tag{10a}$$

$$\text{lengths} \quad X = x/L,\ Y = y/L,\ Z = z/L. \tag{10b}$$

For uniform mass density (ρ = const.), e.g. for low dopant or solute concentrations, or similar molecular weight of all components in the nutrient, (3) can be simplified. With $\nabla\rho = 0$, from (2) $\nabla \cdot v = 0$. Hence $\nabla \cdot \rho_i v = v \cdot \nabla\rho_i + \rho_i \nabla \cdot v = v \cdot \nabla\rho_i$. Substitution of the dimensionless ratios (10) into the thus simplified form of (3) and using $\rho_i/\rho = W_i$, results in

$$U \cdot \nabla W_i = \frac{1}{N_{Pe}} \nabla^2 W_i, \tag{11}$$

where $N_{Pe} = U_0 L/D_{AB}$ is the dimensionless *Peclet number* which signifies the relative weight of convective and diffusive mass flux.

Let us apply the Peclet number concept to the diffusive–convective transport at and across an interface. For this purpose we set the characteristic length L equal to the width δ_c of the interfacial nutrient zone of significant concentration changes (see fig. 1b). Depending on the convective stirring conditions in the bulk nutrient, δ_c may range from a narrow layer at the interface (a "boundary layer") to a characteristic dimension of the nutrient container. The choice of a characteristic velocity in this concentration transition region takes some careful consideration. In general, as schematically indicated in fig. 2 for a binary system, the component fluxes and, thus, v can have any direction

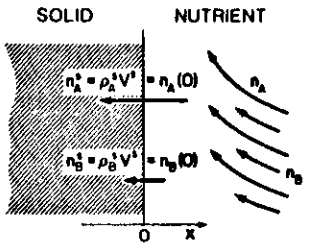

Fig. 2. Component fluxes in diffusive–convective mass transport near planar crystal–nutrient interface in stationary interface frame.

with respect to the interface. *On* the interface, however, we know that due to the no-slip condition, *tangential* velocity components vanish. Hence, we will simplify the situation and consider for this semi-quantitative discussion only velocity components normal to the (stationary) interface. The characteristic velocity in N_{Pe} is then the sum of the advective velocity $v_a(x)$ and the normal component $v_n(x)$ of the (forced or free) convection velocity. The magnitude of both contributions depends in general on the distance x from the interface. (For example, for the "purely diffusive" case, where $v_a = v$, we see from (6) that v_a is proportional to the weight fraction $W_A(x)$.) For not too large variation of $W_A(x)$ in the interfacial region, however, we can approximate $v_a(x)$ with its value on the interface, $v_a(0)$. Then

$$v = v_a(0) + v_n(x) = \frac{\rho^s}{\rho^f(0)} V^s + v_n(x). \tag{12}$$

The $v_a(0)$ is correlated in (12) to the linear growth rate V^s via the density of the crystal ρ^s and the *total* density of the fluid at the interface $\rho^f(0)$, irrespective of the magnitude of segregation (e.g. solution growth, etc.) (see ref. [3], p. 282). But (12) still contains the x-dependent convective velocity v_n! To circumvent this difficulty, $v_n(x)$ in (12) is traditionally ignored and only the interfacial flow velocity $v(0)$ taken into account. This has its historic root in work by Nernst (1904) [7] who (besides ignoring the $1/(1 - W_A)$ term in (8)) believed in the existence of an "unstirred layer" of macroscopic dimensions at solid–liquid interfaces. This, of course, violates fundamental fluid dynamic principles. On the other hand one may be tempted to argue for a $v_n = 0$ in the interfacial region since "close to an interface diffusion is the dominant mass transfer mode". There is nothing wrong with this qualitative statement. Yet, *how close* to the interface must one go to make the above claim valid? This can be estimated based on the Peclet number

$$N_{Pe} = \frac{V_{cf}\delta_c}{D_{AB}} + \frac{v_n \delta_c}{D_{AB}}, \tag{13}$$

where we have used the abbreviation $V^s\rho^s/\rho^f(0) \equiv V_{cf}$ for the interfacial flow velocity $v(0)$, called crytallization flow by Wilcox [5]. The first term o the rhs represents the relative strength of the a vective and diffusive fluxes towards the interfac the second term is the ratio of the external caused convective flux to the diffusive flux. Fro (13) one sees that the key parameter for the dec sion of whether ignoring v_n is physically realistic the characteristic diffusion distance $Y' = D_{AB}/V$ and not simply the condition $v_n \ll V_{cf}$. The characterizes the distance over which diffusion ca propagate the concentration perturbation from it terfacial segregation, *against* the advective inflo of bulk nutrient due to the interfacial flow. $Y' \approx \delta_c$, then diffusion–advection dominates withi the concentration transition zone δ_c and the n glect of (the typically unknown) v_n is of litt consequences.

If, however, $Y' > \delta_c$ then the concentration pr file at the interface is governed by diffusive-(force convective fluxes. In such cases one may still d cide, for mathematical convenience, to ignore i.e. to replace the actual diffusive–convecti situation by a "diffusion-only" model within "diffusion boundary layer" or "stagnant layer Obviously the width δ_c' of this fictituous layer mu be smaller than the actual δ_c so that t diffusive–advective fluxes in the model can resu in the same transport rate as the diffusive–conve tive mechanism in the real system. Unfortunatel the great convenience of this model has caus many workers to confuse it with "the real thing Though stagnant layer models give, through t definition of the layer thickness, the correct inte facial fluxes, one cannot expect that they yie realistic concentration profiles for $\delta_c \ll Y'$ a consequently $\delta_c' \ll \delta_c$.

In table 1 we have evaluated characteristic di fusion distances for representative nutrient-grow

Table 1
Characteristic diffusion distances $Y' = D_{AB}/V_{cf}$ for typi growth rates and diffusion coefficients in various nutrients

Nutrient	D_{AB} (cm²/s)	V^s (cm/h)	$\rho^s/\rho^f(0)$	Y' (cm)
Melt	10^{-4}	1–10	1	0.4–0.04
Solution	10^{-5}	0.04	3	0.3
Vapor	2×10^{-1}	0.04	10^3	20

ate combinations. From these samples it becomes lear that convection cannot be ignored in interfa- ial transport flux descriptions if the concentration ransition zones found in a system are equal to or iarrower than a few mm for melts and solutions, ind several cm in vapors, respectively.

In many real systems $\delta_c < Y'$, i.e. convective nass transport within the distance Y' from the nterface is significant. Then results for the "diffu- ion boundary layer width" obtained in segrega- ion studies, for instance, from the Burton–Prim–Slichter (BPS) relation [8]

$$k_{eff} = \frac{k_0}{k_0 + (1 - k_0)\exp(-\delta_c' V^{cf}/D_{AB})} \quad (14)$$

nust be understood as the entities they were con- ceived to be: as fitting parameters that give the correct numerical result for k_{eff} in a mathemati- cally more tractable model in which convective nass transfer close to the interface is ignored. Several authors have obtained more rigorous solu- ions to segregation problems [9–12]. They have olved the diffusion equation (3) together with the Navier–Stokes equation (1) for (rotating disc) in- erfaces. It must be pointed out, however, that nly the apparently little known work by Sparrow ind Gregg [9] covers the whole Schmidt number (N_{Sc}) range (see eq. (21)). The more recently ob- ained solutions [10–12] are limited to $N_{Sc} \gg 1$, vhich, as we will see below, limits them to liquid ystems with marginal applicability to silicon. These results have shed considerable light on the actual meaning of δ_c and δ_c'. Yet, it is often ignored hat these solutions (including eq. (14)) are based on ρ = constant, i.e. on low concentrations of the olute. This restricts them to the impurity-in-melt ase or extremely low solute concentration solu- ion growth. With ρ = const. the formal treatment implifies for several reasons: (a) the Navier–Stokes equations can be solved indepen- dently of the actual species distribution; (b) the dvective flux contribution to the convective field an be ignored, i.e. (9) can be used instead of (8); and, as a consequence (c) the convective velocities n the diffusion equation are those independently obtained in (a).

With the rapid development of high speed com- puters and efficient numerical algorithms, the $\nabla\rho = 0$ restriction will soon become unnecessary even for realistic geometries. Thus, solutions to the segregation problem in high concentration systems should become tractable in the near future.

Fortunately, considerable insight on concentration distributions of specific problems can be obtained from analogies to the corresponding velocity and temperature fields. These are experimentally more readily accessible and have been treated more extensively in the transport literature.

3.3. Similarities between momentum and species transport

For a comparison of momentum and concentration transport at interfaces we will now "non-dimensionalize" the Navier–Stokes equation (1) in the same manner as the diffusion equation (3) in section 3.2. In addition to the dimensionless velocity and length ratios (10) we use a characteristic pressure p_0 to express a dimensionless pressure as

$$P = p/p_0. \quad (15)$$

Substitution of (10) and (15) into the steady-state form of (1) for negligible body forces yields

$$U \cdot \nabla U = \frac{p_0}{\rho U_0^2}\nabla P + \frac{1}{N_{Re}}\nabla^2 U, \quad (16)$$

where $N_{Re} = U_0 L/\nu$ is the dimensionless *Reynolds number*. In most (crystal growth) flow configurations the first term on the right-hand side of eq. (16) can be ignored. Hence, we recognize N_{Re} as the ratio of inertial to viscous forces in a given flow.

Note the similarity of the simplified (16) with the non-dimensional convective-diffusion equation (11). From this similarity we can expect that in a given configuration with similar boundary geometry for velocity and concentration, solutions to the species distribution can be obtained by scaling through N_{Re} and N_{Pe}. We will illustrate this with three configurations relevant to crystal growth, in which the bulk flow is directed parallel to the interface and undergoes momentum and species exchange with that lateral boundary.

Flow near a rotating disk is encountered, for

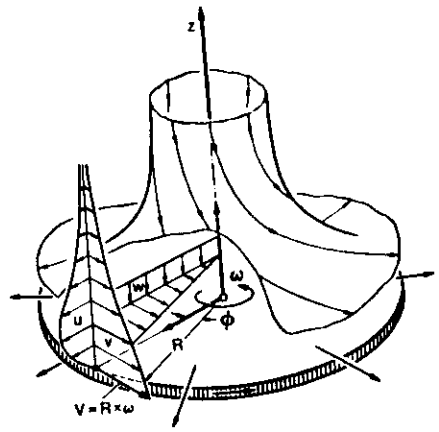

Fig. 3. Flow near a disk rotating in a fluid at rest. After ref. [13].

instance, in pulling from the melt. As shown in fig. 3, a layer near the rotating disk is carried by it through friction and is thrown outward due to the centrifugal forces acting upon it. This outward flow is balanced by an axial flow towards the disk to be in turn carried and ejected centrifugally. The solution of (1) for this problem [14] reveals that the width of the transition zone in which the axial velocity attains its bulk value is independent of the distance from the rotation axis. For instance, 99% of the limiting bulk value are reached within a distance δ_v from the disc, frequently called "momentum boundary layer", that is given by

$$\delta_v = 4(\nu/\omega)^{1/2}. \quad (17)$$

Another example of an exactly solved flow configuration is the flow parallel to a flat plate that is, for instance, found in epitaxial growth reactors. Fig. 4 illustrates that the width of the zone over which the viscous interaction with the plate causes the flow velocity to change significantly increases with distance from the leading edge, x. A solution of the problem [13] yields for this velocity boundary layer width

$$\delta_v = 5(\nu x/U_\infty)^{1/2}. \quad (18)$$

As a last example for a configuration that also occurs frequently in crystal growth, let us look at the steady flow of a viscous fluid in a conduit of constant cross-section, often referred to as a Poiseuille flow. Fig. 5 shows that in the entrance region of the conduit a velocity boundary layer develops and eventually reaches the center of the pipe from where the velocity profile becomes independent of x. The distance over which this transition to fully developed Poiseuille flow is accomplished, i.e., the entry length l is found to be [15]

$$l = C/\nu, \quad (19)$$

where C depends on the free flow velocity U_0 and the cross-section (radius) of the tube.

These examples well identify the kinematic viscosity of the fluid as the governing parameter for momentum transport. The higher ν the farther into the bulk fluid propagates (diffuses) the perturbation from a momentum boundary. This is in strict analogy to the diffusion of species that is governed by D_{AB}. From this we can conclude that scaling of the coupled velocity and concentration fields can be based on a one-to-one correlation of N_{Re} and N_{Pe}. This has been confirmed by numerous rigorous solutions to specific systems. With respect to the for us most interesting transition zones ("boundary layers") we find that for *similar*

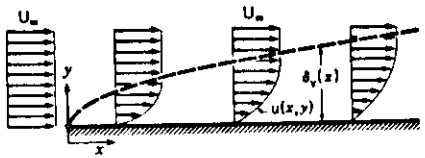

Fig. 4. Development of velocity boundary layer on a flat plate in parallel flow at zero incidence. After ref. [13].

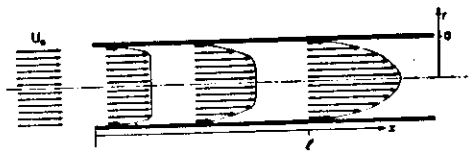

Fig. 5. Definition sketch for the entrance length l in Poiseuille flow.

boundary conditions, constant fluid properties and laminar flow

$$\frac{\delta_v}{\delta_c} \approx C_1\left(\frac{\nu}{D_{AB}}\right)^n = C_1\left(\frac{N_{Pe}}{N_{Re}}\right)^n. \qquad (20)$$

For the geometrical constant C_1 and exponent n one can expect, from the above solutions to momentum transfer problems, values of order unity and around 1/2, respectively. Rigorous solutions show that n is weakly dependent on ν/D_{AB} with $1 \geq n \geq 1/3$ for $0 \leq \nu/\kappa \leq \infty$ [9,16,17]. The similarity implied here requires, e.g., in the parallel flow case that the plane is a momentum boundary *and* a surface of fixed concentration, and the free flowing fluid must possess some other fixed bulk concentration.

From the above we see that the dimensionless ratio of Peclet number and Reynolds number, known as the *Schmidt number*

$$N_{Sc} = \frac{N_{Pe}}{N_{Re}} = \frac{U_0 L}{D_{AB}} \frac{\nu}{U_0 L} = \frac{\nu}{D_{AB}}, \qquad (21)$$

well approximates the relative weight of momentum and mass diffusion. By inserting typical values for ν and D_{AB} into (21) we obtain a characteristic difference between gases and liquids, see table 2. Whereas N_{Sc}'s for gases range between 0.1–1, with the majority around unity, most liquids possess Schmidt numbers of 10 and higher. Thus, as schematically indicated in fig. 6a, in gases the concentration and velocity profiles extend about the same distance into the bulk nutrient, independent of the free stream velocity. In liquids, however, δ_v exceeds δ_c considerably (fig. 6b). Thus, in regions of major concentration change at the interface the flow velocity is reduced to relatively small values.

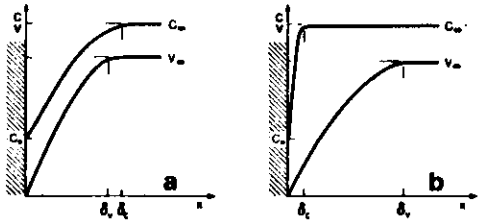

Fig. 6. Schematic comparison between concentration and velocity distributions at solid–fluid interfaces for fluids of small and large Schmidt numbers: (a) $N_{Sc} \leq 1$ (gases); (b) $N_{Sc} \gg 1$ (liquids).

The practical implications of fig. 6 are numerous. For instance, it is obviously meaningless to discuss interfacial mass transport in vapor crystal growth in terms of "diffusion-only" models unless one is fully aware of the fictitious nature of that approach. This was already anticipated in the discussion of the effective diffusion length (table 1). Also, one can expect that changes in the convection behavior (and, hence, in the interfacial velocity profile) in vapor growth are particularly prone to lead to compositional inhomogeneities.

3.4. Similarities between energy and species transport

For a comparison between interfacial heat, species and momentum transfer we will follow the above "recipe" and non-dimensionalize the energy transport equation (4). With some reasonable simplifications we obtain

$$U \cdot \nabla T = \frac{1}{N_{Pe}^T} \nabla^2 T, \qquad (22)$$

where $N_{Pe}^T = U_0 L/\kappa$ is the *thermal Peclet number*, that characterizes the relative weight of convective and conductive (diffusive) heat fluxes. The "generalized diffusion coefficient" for heat is the thermal diffusivity $\kappa = k/\rho C_p$.

From the similarity of (22) to the dimensionless transport equation for momentum (16) we can expect that a relation between a thermal transition zone width δ_t and δ_v can be written as

$$\frac{\delta_t}{\delta_v} \approx C_2\left(\frac{\kappa}{\nu}\right)^n = C_2\left(\frac{N_{Re}}{N_{Pe}^T}\right)^n, \qquad (23)$$

where C_2 is about unity. The exponent n depends again only weakly on ν/κ, approaching $n = 1/3$ for $\nu/\kappa \gg 1$ and $n \to 1$ for $\nu/\kappa \to 0$. Thus, the ratio ν/κ, known as *Prandtl number*, N_{Pr}, signifies the relative strength of heat and momentum flux.

In evaluating (23) for specific fluids, one finds that one cannot simply distinguish again between liquids and gases; see table 3. As schematically indicated in fig. 7a, in liquid metals and semiconductors the thermal boundary layer δ_t usually extends three times further into the melt than the velocity transition region. However, in molten oxides and aqueous solutions δ_v is somewhat wider than δ_t. In gases, on the other hand with a typical $N_{Pr} \approx 0.7$, δ_t and δ_v must have comparable values. Similarly one can conclude that in gas flows (CVD reactors) the thermal and velocity entrance lengths must be about equal. Thereby one assumes, of course, that the momentum boundary is also a constant (high) temperature surface, which may not be the case in actual CVD reactors [18].

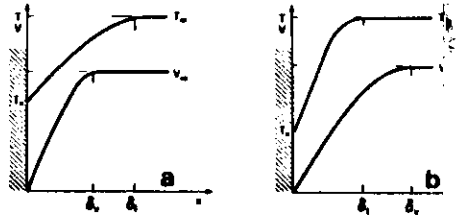

Fig. 7. Schematic comparison between velocity and temperature distribution at solid–fluid interfaces for different groups: (a) $N_{Pr} \ll 1$ (liquid metals, semiconductors); (b) $N_{Pr} \gg 1$ (aqueous solutions, molten oxides).

At last, comparing interfacial mass and heat transfer, we deduce from (11) and (22) that similarly to (23)

$$\frac{\delta_t}{\delta_c} \approx C\left(\frac{\kappa}{D_{AB}}\right)^n = C\left(\frac{N_{Pe}}{N_{Pe}^T}\right)^n, \qquad (24)$$

where the ratio of heat and mass flux strength $N_{Pe}/N_{Pe}^T = N_{Sc}/N_{Pr}$ is often referred to as the *Lewis number*, N_{Le}. Here we can consider gases and liquids again as distinctly differently behaving fluids. With gases, where representative values for κ and D_{AB} are both around 0.7 cm²/s, temperature and concentration profiles extend over comparable distances from a solid–vapor interface into the nutrient (fig. 8a). This, of course, is in excellent accord with kinetic gas theory which yields the same value for the self-diffusion coefficient as

Table 2
Approximate values [3] of kinematic viscosities, diffusion coefficients and resulting Schmidt numbers for various fluids

Fluid	Temperature (C°)	Pressure (Torr)	ν (cm²/s)	D_{AB} (cm²/s) (diffusant)	$N_{Sc} = \nu/D_{AB}$
Hydrogen	1000	760	12	~18 (CO_2)	0.7
Air	0	760	0.13	0.2 (H_2O)	0.6
Water	25		10^{-2}	1.6×10^{-5} ($NaCl$)	6×10^{2}
KBr	780		7×10^{-3}	4.9×10^{-5} (Ag^+)	$\approx10^{2}$
Ga	30		3×10^{-4}	2×10^{-5}	15
Si	1420		4×10^{-3}	7×10^{-4}	5.7
GaAs	1240		3×10^{-3}	1.2×10^{-4}	25
Al_2O_3	2100		0.3	2.2×10^{-4}	1400

Table 3
Approximate values of kinematic viscosities, thermal diffusivities and resulting Prandtl numbers for various fluids (after ref. [3])

Fluid	Temperature (°C)	ν (cm²/s)	κ (cm²/s)	$N_{Pr} = \nu/\kappa$
Hydrogen	1000	11.6	16.9	0.68
Air	50	0.18	0.26	0.71
Water	0	1.8×10^{-2}	$\approx10^{-3}$	15
	50	5.5×10^{-3}	$\approx10^{-3}$	6
Zinc	420	4.4×10^{-3}	0.2	2.2×10^{-2}
Silicon	1430	0.13	0.03	4×10^{-3}
Al_2O_3	2070	0.35	$\approx10^{-2}$	≈ 40

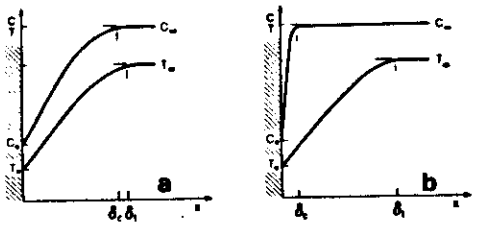

Fig. 8. Schematic comparison between concentration and temperature distribution at solid–fluid interfaces for fluids of small and large Lewis number: (a) $N_{Le} = 1$ (gases); (b) $N_{Le} \gg 1$ (liquids).

the thermal diffusivity of an ideal gas. At liquid–solid interfaces, however, δ_t will always be wider than δ_c. In molten oxides their ratio is smaller than in liquid metals where, due to the high k, δ_t may extend 10 times as far into the fluid as δ_c.

The relations (23) and (24) are particularly useful since they allow for estimates of concentration and velocity profiles at interfaces from the typically much easier to measure temperature profile. Yet is must be emphasized once more that this correlation is based on the full correspondence between the simplified energy transport equation (22) and the species (mass) transport equation (11) *for systems with uniform mass density and fluid properties.*

This analogy is, of course, also observed in situations with vanishing bulk flow (including advective flow). Formally, this is reflected in the mathematical equivalence of Fick's second law $\partial C_A/\partial t = D_{AB}\nabla^2 C_A$ and the heat conduction equation $\partial T/\partial t = \kappa\nabla^2 T$. This mathematical correspondence has led to the custom of deducing solutions to mass transfer problems from solutions to "analogous" heat transfer configurations found in the extensive heat transfer literature. This can be a very efficient approach. Yet in drawing such analogies one must not lose sight of the fundamental difference between diffusive heat and mass transfer. As heat diffuses, neglecting self diffusion, the molecules remain "around" their time-averaged coordinates. Hence the mass-connected reference frame, with respect to which the conductive heat flux is expressed, remains stationary, unless, of course, a convective motion is imposed by external means. As mass diffuses, however, under most circumstances the (same) mass-centered reference frame with respect to which the diffusive mass flux is expressed is moving itself merely due to the diffusive mass flux. This diffusion-induced advective flux (see section 3.2) restricts analogies between "diffusion-only" heat and mass transfer to low solute concentrations in the nutrient.

The reader will have noticed that we have rarely used the popular term "boundary layer" in the foregoing discussion. "Interfacial zone of significant concentration change" is admittedly less concise. Yet the term boundary layer has a specific connotation in fluid dynamics that is often not met in a crystal growth system. For instance, for δ_v to represent a true boundary layer, the $N_{Re} = U_0 L/\nu$ "of the system" (i.e. with L typical for the nutrient extent) must be much larger than unity. Then the flow in the bulk nutrient has only small velocity gradients and, consequently, can be *treated* as if it were inviscid and one can neglect the viscous term in (1). At the interface, however, the velocity changes rapidly over a layer that is narrow as compared to L. For this boundary layer (b–l) region, (1) can again be drastically simplified since only velocity gradients normal to the interface are important. Note that for instance (18) was obtained as a solution to this b–l equation [13] and, thus, holds only for $\delta_v \gg$ L, where the only intrinsic length scale L is given by the distance x from the leading edge ($x = 0$). Corresponding simplified b–l forms of the mass and heat transport equations can be used if the corresponding dimensionless groups $N_{Pe} = U_0 L/D_{AB}$ and $N_{Pe}^T = U_0 L/\kappa$, respectively, are $\gg 1$. In crystal growth, this is often not the case and $N_{Pe} \approx N_{Pe}^T \approx 1$ and therefore $\delta_c \approx \delta_t \approx L$ (see also the use of Y' in section 3.2). If we materials preparation workers are interested in "talking sense" with the fluid dynamics community we should respect their well-established terminology.

4. Non-steady transport in nutrients

Time-dependent crystal growth rates lead, via segregation, to compositional non-uniformities in the solid. The post-growth diffusive dispersion of such inhomogeneities is only practical if the characteristic diffusion time

$$\tau_c = d^2/D_{AB} \tag{25}$$

in the solid is reasonable. Assuming a typical spacing for dopant "striations" of $d = 10$ μm and $D_{AB} = 10^{-16}$ cm²/s (i.e. D_{As} in Si (800°C), ref. [19]), we obtain $\tau_c \geq 10^8$ h! In other words, if $D_{AB} \leq 10^{-12}$ cm²/s and, thus, $\tau_c \geq 10^2$ h, the prevention of non-steady growth becomes crucial.

Let us assume that the externally imposed boundary conditions in a crystal growth process are perfectly stable. Then non-steady growth and segregation can have their origin only in time-dependent convection in the nutrient, or in oscillatory interfacial kinetics [20–23]. Time-dependent free convection, in turn, may arise from surface tension gradients or buoyancy. Our quantitative understanding of oscillatory convection in general and of time-dependent surface tension-driven flow in particular is currently very limited. Hence, we will here only touch on a few practically important trends associated with buoyancy-driven flow in the various groups of nutrients.

The buoyancy-driven convective state of a monocomponent fluid is governed by the *thermal Rayleigh number*

$$N_{Ra} = \beta g h^3 \Delta T/\nu\kappa, \tag{26}$$

the Prandtl number, and the geometry and physical properties of the boundaries. Fig. 9 presents the various flow regimes encountered in a Bénard system with rigid (no-slip) and conducting boundaries. Convection can be sustained when N_{Ra} exceeds a critical value N_{Ra}^c, around 1700 for the above boundary conditions, independent of the specific fluid considered. On the other hand, from (26) and materials parameters of table 3, with typical β-values it follows that the ΔT needed for a specific N_{Ra} in liquid metals, gases, and molten oxides, respectively, is approximately 20, 500 and 1000 times that in water.

From fig. 9 we see that the condition for onset of oscillatory convection, i.e. N_{Ra}^{osc} depends strongly on the fluid's N_{Pr}. For oxide melts, for instance, with $N_{Pr} \approx 40$, the destabilising temperature gradient can be increased to more than 30 times the threshold value (corresponding to N_{Ra}^c) before oscillations set in. In contrast, in semiconductor and metal melts, a slight increase beyond N_{Ra}^c drives the system into oscillations!

Lateral boundaries, as long as they are not associated with horizontal temperature gradients, act convectively stabilizing. The regimes of the various convection states are shifted to higher N_{Ra}'s. Most recent results indicate that, in addition, the regime diagram becomes a great deal more complex. In fig. 10 we have assembled a *semi-quantitative* convection regime diagram for bottom heated, cylindrical columns of fluid with a

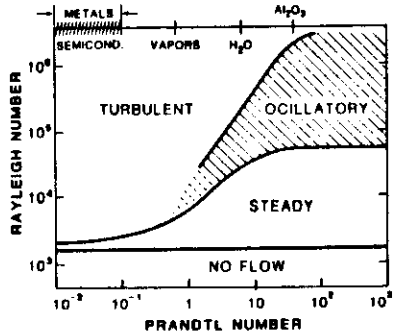

Fig. 9. Regime diagram for expansive (thermal) convection between horizontal, differentially heated planes. After ref. [24].

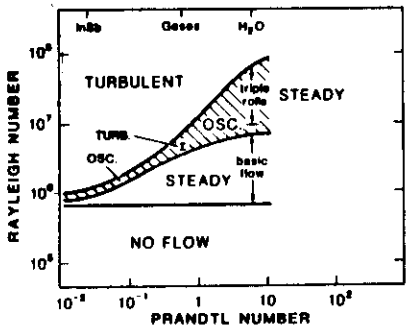

Fig. 10. Convection regime diagram for bottom heated vertical circular and "conducting" cylinder of aspect ratio 10. Semi-quantitative; see text.

height to radius (aspect) ratio of approximately 10. Whereas fig. 9 is based on well defined experiments with numerous different fluids, fig. 10 is based on results for InSb, gases and water only, obtained either for not too well defined thermal boundary conditions or somewhat different aspect ratio. (For a closer evaluation the reader is urged to refer to the original papers [25–29].) Fig. 10 strongly suggests a close spacing of N_{Ra}^{c} and N_{Ra}^{osc} for low N_{Pr} nutrients and a large difference at high N_{Pr}'s also in the presence of lateral confines. Beyond these features that are in common with the Benard geometry, well reproducible turbulent and steady flow regimes have been observed within the oscillatory domain. Of course, the data are yet too limited to attempt any assignments of these new features to groups of N_{Pr}'s.

Considerable efforts have been made to understand the origin of oscillatory transport. For a recent review see ref. [30]. At this point it appears that $N_{Pr} \approx 5$ forms the borderline between two different mechanisms. For high N_{Pr} fluids we have seen in fig. 7b that the momentum transition zone is wider than δ_t. Consequently, as convection sets in, the linear temperature profile of a conduction state is more readily deformed by the flow than in fluids with $N_{Pr} \ll 1$. This trend is schematically indicated in fig. 11 for, say , the temperature profile in the vertical center plane of an individual convection roll. For $N_{Pr} \gg 1$, the temperature gradient in the "core" of the roll is thus sizeably reduced. That causes; in turn the convective streamlines to be more concentrated adjacent to

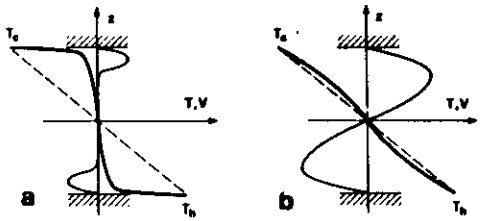

Fig. 11. Schematic temperature and velocity profiles (heavy and light curves, respectively) in the vertical center plane of a convection roll between horizontal planes. (a) $N_{Pr} \gg 1$, (b) $N_{Pr} \ll 1$. Dashed lines represent temperature profile from conduction only.

the ("convection-sustaining") horizontal planes. The flow becomes increasingly confined to the boundary regions. For fluids with $N_{Pr} \ll 1$ (figs. 7a and 11b) quite different behavior can be expected. Since convection contributes to a lesser extent to heat transfer in these flows the linear temperature profile is less deformed upon onset of convection. Consequently, more of the original gradient can remain active for driving the flow over a greater volume of the fluid. Even with further increase in N_{Ra} (or ΔT, for that matter) the flow maintains more of a bulk circulatory character.

As a consequence of this different flow behavior, (oscillatory) instabilities originate in different regions of the flow. In high-N_{Pr} fluids it is a gravitational boundary layer instability that leads to oscillations. Buoyant fluid accumulates at the heating boundary and grows until a local critical N_{Ra} is exceeded. (The same argument applies, of course, to the cooling upper boundary.) Then "thermals" or "plumes" break away and rise, or sink, respectively. The period after breakaway until a new thermal begins to form is observed to be short as compared to the "growth time". Hence the periodicity will essentially be governed by the thermal diffusion time

$$\tau_\kappa = d^2/\kappa, \tag{27}$$

where d is comparable to the thermal boundary layer width.

For low N_{Pr} fluids one expects from the above that oscillatory instabilities result from a "bulk mechanism" rather than a boundary layer instability. Nonlinear analysis confirms this expectation [30] and yields periods of the order of the viscous diffusion time

$$\tau_\nu = d^2/\nu. \tag{28}$$

Evaluation of (27) and (28) in their respective regimes yields frequencies of the order of s to min for both mechanisms. A distinguishing feature, however, is the proportionality between the square of the frequency and N_{Ra} for the bulk meachnisms, which can be used for identification. This is convenient since low N_{Pr} fluids are in general not transparent and defy visual observation of the flow pattern.

Finally, let us apply dimensionless analysis to a distinction of the flow velocities expected for the two groups of fluids with $N_{Pr} \gg 1$ and $N_{Pr} \ll 1$. We know that convection sets in at the same N_{Ra}, independent of N_{Pr}. We can rewrite the N_{Ra} of (26), however, as a product of N_{Pr} and the *Grashof number*,

$$N_{Ra} = N_{Pr}\, N_{Gr} = \frac{\nu}{\kappa}\,\frac{\beta g h^3 \Delta T}{\nu^2}, \tag{29}$$

where N_{Gr} represents the dimensionless product of the ratios of buoyant to viscous forces and inertial to viscous forces,

$$N_{Gr} = F_b F_{in}/(F_{vis})^2. \tag{30}$$

From this we can deduce that for very low N_{Pr} the N_{Gr} must be much higher than for $N_{Pr} \gg 1$, to get the same N_{Ra}. Higher N_{Gr} scales with a higher intertial term and, thus, higher flow velocities. This qualitative expectation is well confirmed by experimental results. Up to two orders of magnitude higher flow velocities can be expected in, say, liquid metals as compared to molten oxides for the same N_{Ra}.

The difference in flow patterns and velocities of the low and high N_{Pr} groups of fluids has various practical implications. For instance, the resulting mixing behavior in melts can be expected to be quite different. Also, the surface roughness of a container (presence of crystallites, etc.) will have a quite different influence on the convective stability of the fluid. Surface roughness can be important for high-N_{Pr} fluids where the flow is concentrated in a boundary layer. For low-N_{Pr} fluids, however, where the flow is more distributed throughout the bulk, surface roughness will be of little influence.

5. Summary

Rigorous modeling of heat and mass transfer in multicomponent crystal growth fluids is often unwieldy. Consequently, numerous simplifying models have been used in the materials preparation literature. Though well justified for certain special cases, indiscriminate application of these simplifications has caused much confusion. In particular, boundary layer concepts fall into this category. On the other hand, scaling based on dimensionless groups of fluid properties and characteristic dimensions can give practically valuable insight on concentration and temperature distributions in crystal growth arrangements. Such a parametric comparison facilitates the exploitation of similarities in the fluid dynamic behavior of seemingly disparate nutrients.

Acknowledgements

We would like to express our appreciation for conceptual clarifications on the draft of this paper by D.T.J. Hurle, G.H. Westphal, and W.R. Wilcox. Also, support by the National Science Foundation (Grant DMR 79-13183) and the National Aeronautics and Space Administration (Grant NSG-1534), as well as by the Bundesministerium für Forschung und Technologie is gratefully acknowledged.

Nomenclature

C_0^s	Dopant molar concentration in solid near interface
C_0^n	Dopant molar concentration in nutrient near interface
C_∞^n	Dopant concentration in the bulk nutrient
C_p	Specific heat at constant pressure
D_{AB}	Binary diffusivity
g	Acceleration of gravity
k	Thermal conductivity
k_0	Interfacial segregation coefficient, C_0^s/C_0^n
k_{eff}	Effective segregation coefficient, C_0^s/C_∞^n
L	Characteristic distance
n_i	Total (diffusive + convective) component mass flux
p	Hydrostatic pressure
q	Conductive heat flux
u	Internal energy density
U	Dimensionless mass average velocity
U_0	Characteristic velocity
v	Mass average velocity
v_i	Component velocity
W_i	Mass fraction of component i, ρ_i/ρ

x Coordinate normal to interface into fluid
β Thermal expansion coefficient, $(1/V_0)\,\partial V/\partial T$
η Viscosity
κ Thermal diffusivity, $k/\rho C_p$
ν Kinematic viscosity, η/ρ
ρ Total mass density
ρ_i Component mass density
τ Stress tensor
ω Angular velocity

References

[1] R.B. Bird, W.E. Stewart and E.N. Lightfoot, Transport Phenomena (Wiley, New York 1960) ch. 16.
[2] W.R. Wilcox, in: Preparation and Properties of Solid State Materials, Vol. 2, Ed. W.R. Wilcox (Dekker, New York, 1976) p. 129.
[3] F. Rosenberger, Fundamentals of Crystal Growth I (Springer, Berlin, 1981).
[4] J. Stefan, Ann. Physik Chem. 17 (1882) 555.
[5] W.R. Wilcox, J. Crystal Growth 12 (1973) 93.
[6] G.H. Westphal and F. Rosenberger, J. Crystal Growth 43 (1978) 687.
[7] W. Nernst and E. Brunner, Z. Physik. Chem. 47 (1904) 52, 56.
[8] J.A. Burton, R.C. Prim and W.P. Slichter, J. Chem. Phys. 21 (1953) 1987.
[9] E.M. Sparrow and J.L. Gregg, J. Heat Transfer 82 (1960) 249.
[10] L.O. Wilson, J. Crystal Growth 44 (1978) 247 and 371.
[11] J.-J. Favier and L.O. Wilson, J. Crystal Growth 58 (1982) 103.
[12] D. Camel and J.-J. Favier, J. Crystal Growth 61 (1983) 125.
[13] H. Schlichting, Boundary Layer Theory (McGraw-Hill, New York, 1968).
[14] W.G. Cochran, Proc. Cambridge Phil. Soc. 30 (1934) 365.
[15] H.S. Lew and Y.C. Fung, J. Biochem. 3 (1970) 24.
[16] V.G. Levich, Physicochemical Hydrodynamics (Prentice-Hall, Englewood Cliffs, NJ, 1962) sections 10 and 11.
[17] W.R. Wilcox, in: Preparation and Properties of Solid State Materials, Vol. 1, Ed. R.A. Lefever (Dekker, New York, 1971) pp. 77ff.
[18] L.J. Giling, J. Electrochem. Soc. 129 (1982) 634.
[19] D. Shaw, Ed., Atomic Diffusion in Semiconductors (Plenum, London, 1973).
[20] C.J. Allègre, A. Provost and C. Jaupart, Nature 294 (1981) 223.
[21] J.J. Favier, in press.
[22] E. Fitzer, Chem. Ing. Tech. 41 (1969) 331.
[23] W. Fritz, High Temp. High Pressure 2 (1970) 291.
[24] R. Krishnamurti, J. Fluid Mech. 60 (1973) 285.
[25] G. Müller, in: Convective Transport and Instability Phenomena, Eds. J. Zierep and H. Oertel, Jr. (Braun, Karlsruhe, 1982) p. 441.
[26] G. Müller and G. Neumann, in: Proc. 4th ESA Symp. on Materials Science under Microgravity, Madrid, 1983, p. 285.
[27] G. Müller, Advan. Space Res. 3 (1983) 51.
[28] J.M. Olson and R. Rosenberger, J. Fluid. Mech. 92 (1979) 609.
[29] J.R. Abernathey and F. Rosenberger, Physica D. submitted.
[30] F.H. Busse, in: Convective Transport and Instability Phenomena, Eds. J. Zierep and H. Oertel, Jr. (Braun, Karlsruhe, 1982) p. 149.